JOURNAL OF CATALYSIS 93, 256–269 (1985)

Fischer–Tropsch Synthesis on Bimetallic Ruthenium–Gold Catalysts

A. K. DATYE[1] AND J. SCHWANK[2]

Department of Chemical Engineering, The University of Michigan, Ann Arbor, Michigan 48109

Received June 8, 1984; revised January 8, 1985

The effect of Au in the behavior of Ru as a Fischer–Tropsch catalyst was studied. Two series of catalysts were investigated, one supported on SiO_2 and the other on MgO. Au did not seem to alter the product distribution on Ru at pressures up to 1 MPa and in the temperature range 490–570 K. However, the turnover frequencies for both CO hydrogenation and methanation showed a precipitous drop with the Au content in the SiO_2-supported catalysts, whereas on the MgO series a maximum in activity was observed at an intermediate Au content. These activity patterns were correlated with extensive physical characterization placing major emphasis on analytical electron microscopy. The activity trends as a function of Au content were remarkably similar to those previously reported for the structure-sensitive ethane hydrogenolysis reaction. In both reactions, the effect of Au appears to be due to a dilution of the active Ru ensembles.

INTRODUCTION

While Ru is one of the most active catalysts for the CO hydrogenation reaction (*1*), it has not found significant commercial application as a Fischer–Tropsch catalyst (*2*). One disadvantage is its higher cost compared to Fe or Co which are commonly used as Fischer–Tropsch catalysts. Nevertheless, it's catalytic behavior is quite interesting. For example, a large yield of high-molecular-weight waxes can be obtained at low temperatures and high pressures. In contrast to Fe, the yield of oxygenates on Ru is relatively low. Thus, there is a strong motivation to study the behavior of Ru and to explore the effects of promoters or additives on product selectivities.

We chose to investigate the Ru–Au system in view of the interesting behavior of Au in terms of its interaction with catalyst support materials (*3–6*). A particularly intriguing aspect of this interaction is the increased mobility of support oxygen found in isotopic oxygen exchange experiments on Au/MgO (*7*). One objective of this study was to explore whether this oxygen mobility in the MgO support would influence the selectivity toward oxygenates.

Second, catalysts that do not dissociate CO, such as Pd, yield predominantly methanol while Ru which can dissociate CO under reaction conditions catalyzes the chain growth yielding mainly oxygenate-free products (*8*). Adsorption of CO on group Ib metals, such as Au, is weak and reversible and involves a molecularly adsorbed linear CO species (*9, 10*). The availability of weakly held undissociated CO on Au adjacent to active Ru sites might play a similar role to that of CO on Pd. Further, the most widely used methanol synthesis catalyst involves another group Ib metal, namely Cu/ZnO. It has been suggested that the active form of the catalyst involves an oxidized state where the Cu species interact electronically with ZnO (*11, 12*). In the Au/MgO system, EXAFS results gave evidence for the existence of a highly dispersed Au/MgO phase with a formal Au oxidation state of +1 (*3*), thus making it interesting to study the effect of this electronically interacting Au species as a promoter.

[1] Present address: Department of Chemical and Nuclear Engineering, University of New Mexico, Albuquerque, N.M. 87131.

[2] To whom correspondence should be addressed.

0021-9517/85 $3.00

The Ru–Au system contains two metal components which are immiscible in the bulk state. In previous work (*5, 13*), evidence for interactions between the two metal components was found despite their bulk immiscibility. For instance, in the structure-sensitive ethane hydrogenolysis reaction, Au exerted a massive influence on the catalytic activity of Ru. Au by itself has no detectable activity for either ethane hydrogenolysis or CO hydrogenation under typical reaction conditions. In view of the large characterization data base already available for these catalysts (*5, 10, 13, 14*), we perceived a unique opportunity to compare the activity patterns in the Fischer–Tropsch synthesis with the ethane hydrogenolysis activities reported earlier.

Such a comparison would provide additional information concerning the structure-sensitivity of Fischer–Tropsch synthesis. The evidence on this issue appears to be somewhat contradictory. Single-crystal studies on Ni and Ru surfaces showed no change in methanation turnover number when different crystal planes were exposed to the gas phase, while the ethane hydrogenolysis activities were markedly different, depending on the crystal plane (*15, 16*). On supported catalysts, Bond and Turnham (*17*) working with Ni–Cu and Luyten *et al.* (*18*) working with Ru–Cu observed a drop in the methanation activity with increasing Cu content similar to the patterns in ethane hydrogenolysis reported by Sinfelt (*19, 20*). The single-crystal studies suggest that the methanation is insensitive to the structure of the crystal surface. However, the different results on the supported catalysts indicate that both hydrogenolysis and methanation reactions respond in analogous fashion to group Ib metal-induced changes on the Ni and Ru catalysts. These changes could be either electronic and/or geometric in nature, and could also be dispersion related. With regard to the effect of dispersion, Kellner and Bell (*21*) found a drop in the methanation turnover number with increasing Ru dispersion while Vannice and Twu (*22*) reported no change in the methanation activity with increasing Pt dispersion. The Ru–Au system offers an opportunity to investigate each of these aspects in detail.

EXPERIMENTAL

Materials. Two series of catalysts were prepared, one supported on SiO_2, the other on MgO. For both catalyst series, the precursor compounds were $RuCl_3 \cdot H_2O$ (Rudi Pont, reagent grade) and $HAuCl_4 \cdot 3H_2O$ (Carlo Erba RPE). The support materials were Davison SiO_2 (951 N) with a surface area of 650 m^2/g and Carlo Erba MgO (RPE-ACS) with a surface area of 15 m^2/g. Both catalyst series were prepared using aqueous solutions of the metal precursors and standard impregnation techniques. The details of catalyst preparation are described elsewhere (*5, 13*).

For catalyst pretreatment, hydrogen (Air Products, prepurified) and helium (Air Products, high purity) were used. For the Fischer–Tropsch reaction, a gas mixture containing 25.2 vol% CO in H_2 (Matheson, premixed) was further purified by passing it through a MnO/SiO_2 oxytrap (*23*) and a molecular sieve 5A trap.

Characterization. Each catalyst was assigned a code letter: "R" for Ru, "S" for the support material, SiO_2, "M" for MgO, and a three-digit number representing the approximate atomic percentage of Ru. The metal content of the catalysts was determined by atomic absorption spectroscopy. The Ru metal dispersion in the bimetallic samples was determined by H_2 and O_2 chemisorption at room temperature (*5, 13*). A summary of these characterization data is presented in Table 1. In more recent work, we have optimized the chemisorption conditions for a H_2/O_2 titration procedure to determine both the Ru as well as the Au dispersions (*24*).

Photoelectron spectroscopy carried out in a PHI system indicated a Ru surface enrichment in the Ru–Au/MgO series, while in the SiO_2 series the surface composition

TABLE 1

Characterization Data for Ru–Au Catalysts

Catalyst code[a]	Support	Analysis by atomic absorption, wt%		Chemisorption	
		Ru	Au	H/Ru	O_2/Ru
RS100	SiO_2	3.86	—	0.26	0.28
RS091	SiO_2	3.32	0.61	0.29	0.28
RS048	SiO_2	1.66	3.47	0.23	0.28
RS014	SiO_2	0.39	4.65	0.30	0.32
RS000	SiO_2	—	4.69	—	—
RM100	MgO	4.44	—	0.071	—
RM089	MgO	3.48	0.81	0.079	—
RM064	MgO	2.12	2.34	0.100	—
RM010	MgO	0.26	4.45	0.146	—
RM000	MgO	—	3.46	—	—

[a] The numerical value in the catalyst code designates the atomic percentage of Ru with respect to the total metal content of the catalyst.

was similar to the bulk (*13*). EXAFS (*3*) and infrared spectroscopy of adsorbed CO (*10*) gave qualitative indications for a possible interaction between Au and the MgO support.

Electron microscopy. Particle size distributions as well as compositions were determined using a JEOL 100CX scanning transmission electron microscope. Samples were supported on holey carbon film mounted on 75-mesh beryllium grids. In the TEM mode employing a side-entry goniometer stage the point resolution is about 0.7 nm. From the TEM pictures the particle size distributions were derived. For elemental analysis of individual particles we first identified a suitable sample area in the TEM mode, and then the microscope was switched over from the TEM mode to the STEM mode allowing thereby microanalysis of individual crystallites by X-ray energy dispersive spectroscopy (EDS). On the JEOL 100CX machine, which is equipped with a LaB_6 emitter, the probe size is about 10 nm. For the elemental analysis of smaller particles we used a VG HB5 machine at the University of Illinois at Urbana-Champaign. The HB5 is a dedicated scanning transmission electron microscope equipped with a field emission gun. The probe size is about 1 nm, thus allowing analysis of particles in the entire size range of interest.

Apparatus and procedure. For the Fischer–Tropsch studies, approximately 100 mg of catalyst was loaded into a stainless-steel U-tube reactor. The reactor temperature was controlled by an Omega Series 4000 controller. A sheathed thermocouple was mounted directly in the reactor so that the tip was in contact with the catalyst bed. Gas flow rates were controlled by a Tylan mass flow controller. All lines and fittings were made of 316 stainless steel. The reactor effluent lines were heated to prevent condensation of products. For product analysis, a Varian 3700 gas chromatograph equipped with a 3-m Porapak R column and a TCD detector was employed. Data analysis was performed with a HP 3390A integrator. By programming the column temperature between 343 and 453 K, products up to C_6 could be detected.

After loading a new sample into the reactor and flushing with helium, the catalyst was reduced in 20 cm^3/min of flowing H_2 at 573 K for 2 hr, followed by 2 hr at 673 K. CO hydrogenation was carried out under differential reaction conditions (less than 5% CO conversion) in a temperature range 490 to 570 K at total pressures of 198 kPa and, for some runs, 1 MPa. A needle valve downstream of the reactor was used to maintain constant reactor pressure for all catalysts irrespective of the amount of sample. The activity was first evaluated after 10 min on stream. Additional samples of the product stream were analyzed every 30 min. Since some deactivation occurred in the course of a run, the catalyst was regenerated in 20 cm^3/min of flowing H_2 at 673 K for 4 hr between individual Fischer–Tropsch runs. In all cases, this regeneration procedure was sufficient to restore catalyst activity.

To determine the olefin/paraffin selectivity at a given temperature, we alternated Fischer–Tropsch runs of 20 min duration

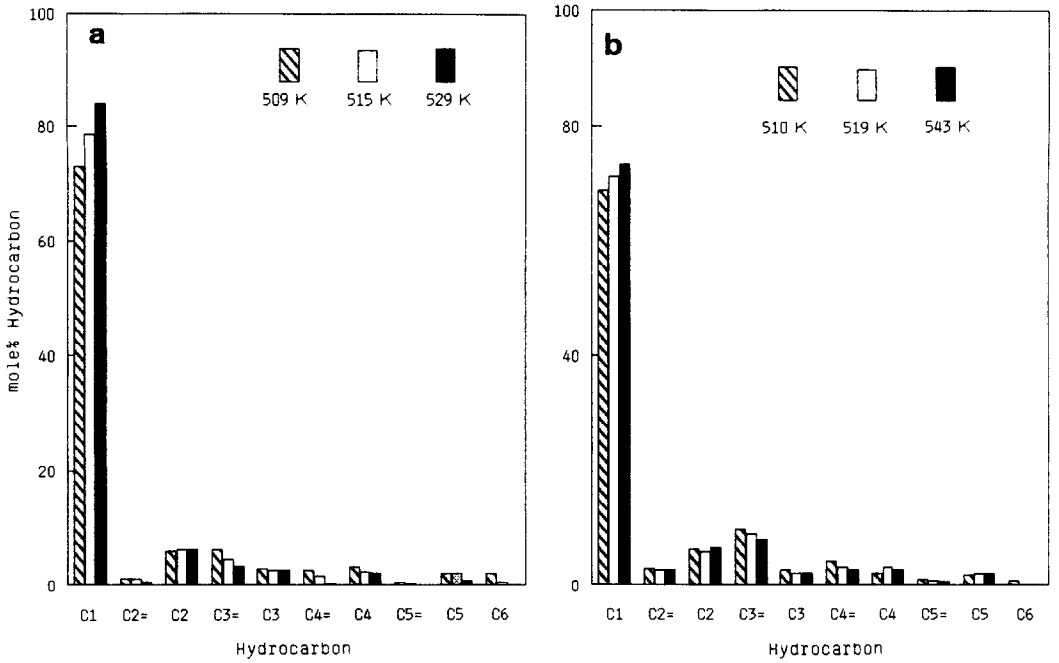

FIG. 1. Product distributions on the SiO_2-supported catalysts. (a) RS100, (b) RS048; $H_2/CO = 3$; pressure = 198 kPa. The symbol = denotes the corresponding olefin product.

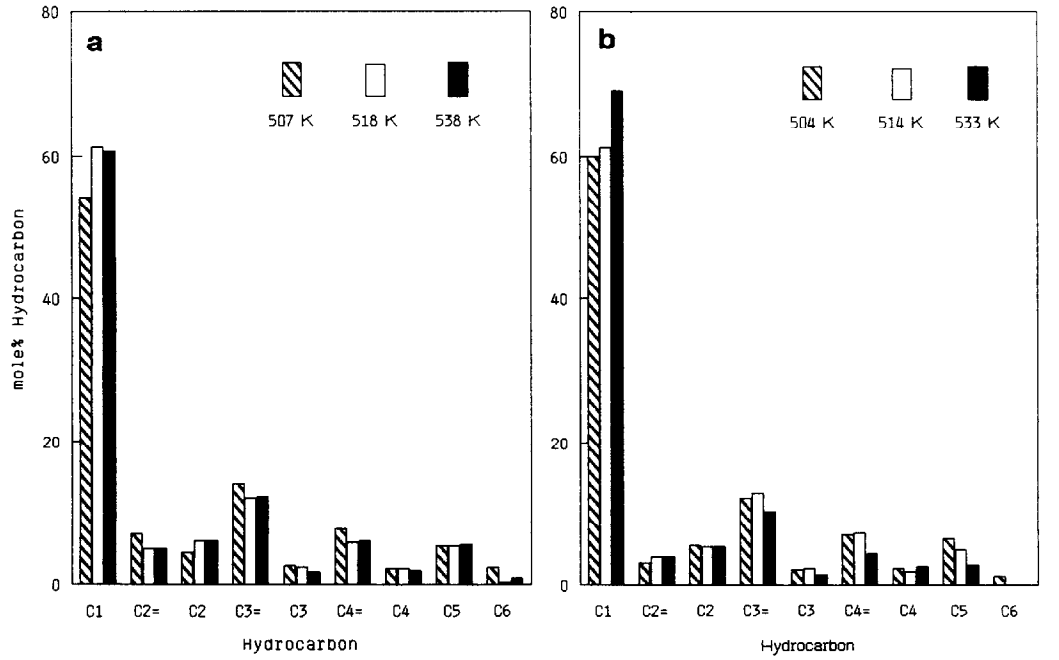

FIG. 2. Product distributions on the MgO-supported catalysts. (a) RM100, (b) RM064; $H_2/CO = 3$; pressure = 198 kPa. The symbol = denotes the corresponding olefin product.

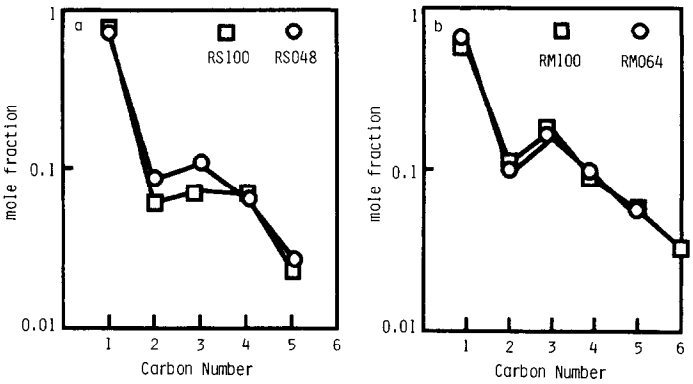

FIG. 3. Schulz–Flory plots for the Ru–Au catalysts. Temperature = 518 K; pressure = 198 kPa; $H_2/CO = 3$. (a) SiO_2 series, (b) MgO series.

with 25-min regeneration periods in flowing H_2 at the reaction temperature. By means of this procedure we were able to study the effect of varying CO conversion on product selectivity with catalyst surfaces that had deactivated to a similar extent.

RESULTS AND DISCUSSION

Catalyst selectivity. The first question to be addressed in this study was the effect of gold on the product distribution in the Fischer–Tropsch synthesis. The product distribution on the SiO_2-supported monometallic RS100 is shown in Fig. 1a while Fig. 1b gives the distribution for the bimetallic catalyst of intermediate composition, RS048. Figures 2a and b show an analogous comparison for the MgO series. The behavior depicted is typical for the other bimetallic catalysts as well. Only the data at 198 kPa have been shown since the influence of Au on Ru at 1 MPa was similar. We have determined products only up to C_6. Higher hydrocarbons were produced, of course, but in such small amounts that it was justified to omit them from the product distributions. With addition of Au to Ru, the relative yields of different hydrocarbons changed only slightly. On the SiO_2-supported catalysts, the selectivity toward methane decreased upon addition of Au to Ru. However, no new products, especially oxygenates, were seen in any of the Ru–Au catalysts. Schulz–Flory plots of the product distributions obtained on catalysts RS100 and RS048 are shown in Fig. 3a. Figure 3b presents the plots for the corresponding catalysts in the MgO series. These plots are representative of the trends seen in all the catalysts and thus, plots for other catalysts have been omitted. All catalysts obeyed more or less the Schulz–Flory product distribution, but there was considerable scatter, especially in the C_2 products. Similar plots for Fe catalysts generally give a much better Schulz–Flory fit compared to Ru (e.g., Ref. (*25*)). There are many instances of similar deviations of Ru catalysts from the Schulz–Flory distribution in the catalytic literature (*1, 21, 26*). One might argue that the relatively high activity of Ru for hydrogenolysis of hydrocarbons contributes via secondary reactions to the observed scatter in the product distribution. If this was indeed the case, one would expect a better fit to Schulz–Flory kinetics on Ru–Au/SiO_2 due to the Au-induced drop in the hydrogenolysis activity of Ru (*13*). However, from Fig. 3, it can be seen that the fit to the Schulz–Flory distribution is not much better in the case of the Ru–Au/SiO_2 catalysts. This is consistent with the findings of Dalla Betta *et al.* (*27*) which show that under CO hydrogenation conditions the hydrogenolysis of higher hydro-

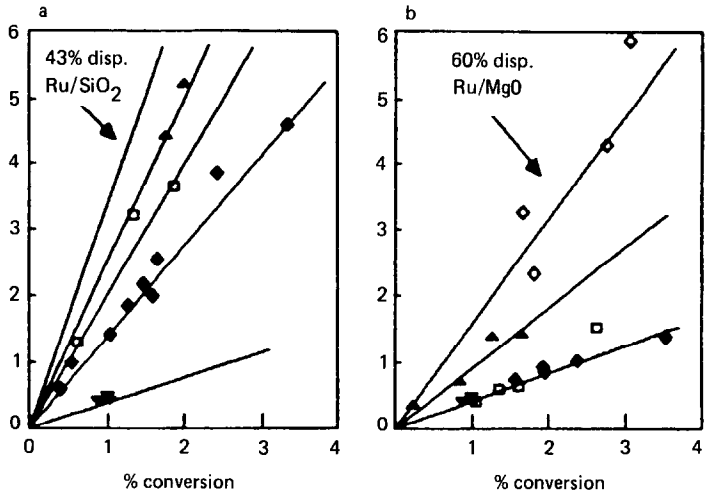

FIG. 4. Paraffin/olefin ratios on the Ru–Au catalysts. Temperature = 518 K; pressure = 198 kPa; $H_2/CO = 3$. (a) SiO_2 series: (□) RS100, (▲) RS091, (♦) RS048, (▼) Ru sponge. (b) MgO series: (□) RM100, (▲) RM089, (♦) RM064, (▼) Ru sponge.

carbons did not contribute significantly to methane formation.

A careful analysis of the olefin/paraffin ratio was conducted to determine whether there was any influence of Au. It is known that the olefin/paraffin ratio changes with CO conversion (*21, 28, 29*). Thus we determined this ratio at various conversions for a given temperature. If the olefin/paraffin ratio is plotted as a function of conversion, we obtain a set of hyperbolas, making direct comparisons between different catalysts difficult. If, on the other hand, one plots the paraffin/olefin ratio, all the points for a given catalyst fall on a straight line passing through the origin (Figs. 4a and b). The fact that all these lines pass through the origin indicates that in the limit of low conversion olefins are the primary products of the synthesis reaction. The slope of this line is an indication of the relative hydrogenation ability of the catalyst. There is no systematic trend apparent between hydrogenation ability and Au content. The differences obtained among the bimetallic catalysts are minor compared to the differences one can obtain by simply varying the dispersion of Ru. To illustrate this, we have also included in Figs. 4a and b the paraffin/olefin behavior of a poorly dispersed Ru sponge and of additional supported monometallic Ru catalysts having higher dispersions. It is obvious that the monometallic Ru catalysts with low and high dispersion bracket the entire bimetallic series on both supports. An effect of dispersion on the olefin/paraffin ratio has also been reported earlier by Kellner and Bell (*21*). They found an effect of Ru dispersion on turnover numbers as well. Both the olefin/paraffin ratio as well as the turnover number dropped precipitously at dispersions exceeding 70%. In our case, the effect of dispersion on the paraffin/olefin ratio can be seen over the entire range of dispersions from 0.1 to 60%.

Since hydrogenation reactions are typically believed to be structure insensitive (*30*), it is surprising to see such a massive influence of metal dispersion on hydrogenation ability. In previous ethane and propane hydrogenolysis studies on these Ru catalysts, we observed an influence of dispersion on the order of reaction with respect to hydrogen (*31*). On the 60% dispersed Ru/MgO catalyst shown in Fig. 4b, the reaction order was −1.93 at a temperature of 458 K, while the poorly dispersed Ru sponge had an order of −1.1 at 461 K. A more negative

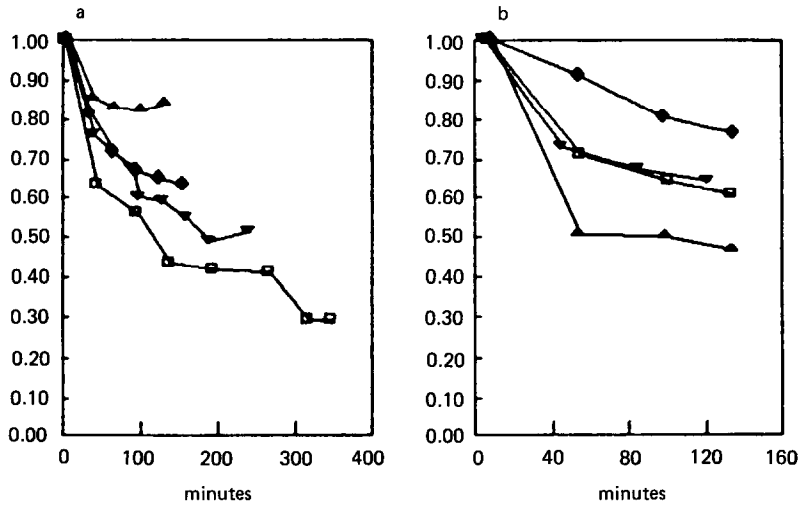

FIG. 5. Deactivation behavior of the Ru–Au catalysts. Pressure = 198 kPa; $H_2/CO = 3$. (a) SiO_2 series: RS100 (□) 518 K and (▲) 504 K; RS048 (♦) 540 K and (▼) 527 K. (b) MgO series: RM100 (□) 538 K and (▲) 507 K; RM064 (♦) 506 K and (▼) 534 K.

reaction order indicates a greater abundance of surface hydrogen and thus one would expect increased ability for hydrogenation in agreement with our observation. One has to keep in mind, of course, that the reaction conditions under hydrogenolysis are vastly different from the conditions encountered in Fischer–Tropsch reactions. Nevertheless, there is a striking similarity in activity patterns seen in both hydrogenolysis and Fischer–Tropsch reactions on our catalysts, as discussed below.

Catalyst activity. Under reaction conditions, a certain degree of deactivation was observed on all our catalysts. Figures 5a and b show the ratio of the actual catalyst activity and the initial activity as a function of time on stream. Ten minutes were more than sufficient to establish steady flows and flush the reactor volume with the reaction mixture. The activity at this time was arbitrarily designated to be the "initial activity." As can be seen from Figs. 5a and b, the drop in activity was most severe in the early stages of the run, followed by a leveling off after about 1 hr on stream. To represent the "steady-state" behavior of the catalyst, we picked arbitrarily the activity after 100 min on stream. All the product distributions and activity patterns reported are the "steady-state" values. Figures 6a and b show the Arrhenius plots for "steady-state" methanation activity as a function of temperature. Apparent activation energies of 100–134 kJ/mol were found which are typical for Ru catalysts. There was no visible systematic influence of Au. However, the preexponential factor varied significantly upon addition of Au (Table 2). Thus, a comparison of turnover frequencies as a function of Au content will give the same activity trends irrespective of temperature over the range studied.

Figure 7 shows the influence of Au on the methanation turnover number at a given temperature. We have also plotted, for comparison, the previously reported activities for ethane hydrogenolysis (*13*). In the SiO_2 series, the turnover numbers of both reactions fall monotonically with increasing Au content. In the MgO series, on the other hand, the activity goes through a maximum at an intermediate Au content. The same overall trends are seen if one plots instead the turnover number for total CO consumption or for the formation of C_2^+ hydrocar-

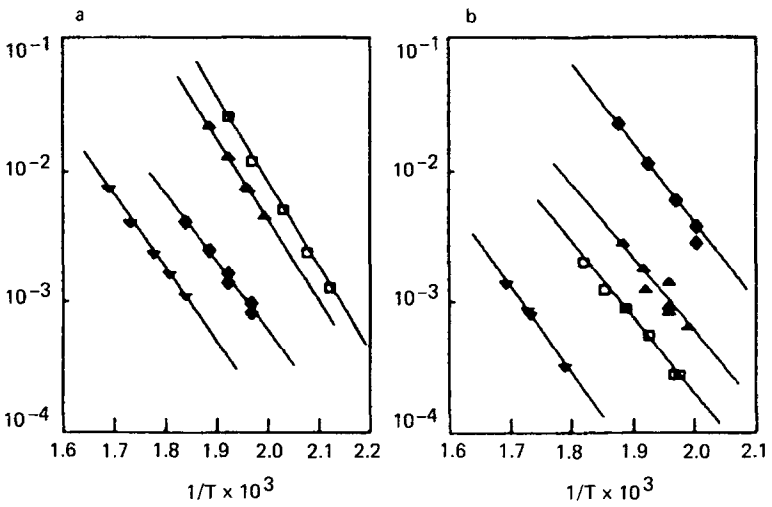

FIG. 6. Specific activities for the formation of CH_4 at 198 kPa and a H_2/CO ratio of 3. (a) SiO_2 series: (□) RS100, (▲) RS091, (♦) RS048, (▼) RS014. (b) MgO series: (□) RM100, (▲) RM089, (♦) RM064, (▼) RM010.

bons (*32*). These trends are definitely not artifacts due to errors in dispersion measurements. For instance, similar activity patterns as seen in Fig. 7 are obtained if one plots the specific activity per gram of Ru instead of the turnover frequency per ruthenium surface atom. It can also be ruled out that the differences introduced by the addition of Au are due simply to differences in deactivation behavior. In Figs. 5a and b, the relative decrease in activity with time on stream is minor compared with the order of magnitude differences seen from one catalyst to another in Fig. 7. Furthermore, Figs. 5a and 6 show no systematic trend on deactivation as a function of Au content.

In order to understand better the differences between the two catalyst series, we

TABLE 2

Kinetic Parameters of the Ru–Au Catalysts in the Fischer–Tropsch Synthesis (Steady-State Activity)

Catalyst code	CH_4		CO	
	E_a[a]	ln (A)[b]	E_a[a]	ln (A)[b]
RS100	125.1	25.2	97.4	19.3
RS091	124.0	24.3	93.0	17.7
RS048	100.0	17.0	92.9	15.8
RS014	104.8	16.4	91.9	13.7
RM100	107.0	17.3	96.5	16.0
RM089	109.0	19.0	93.0	16.0
RM064	134.0	27.0	110.0	22.0
RM010	124.0	18.8	139.0	22.0

[a] Activation energy in kJ/g mol.
[b] A is in molecules/s/site.

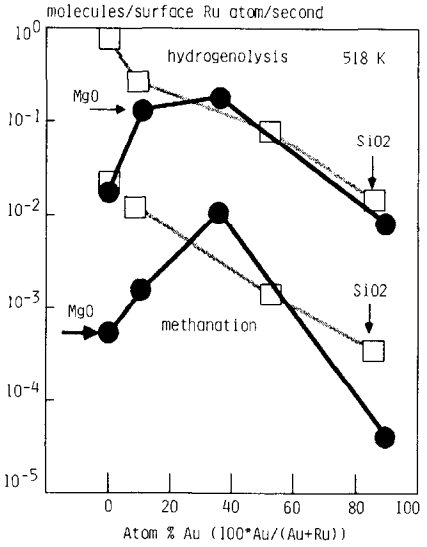

FIG. 7. Effect of Au on the methanation and ethane hydrogenolysis (*13*) activities of the Ru–Au catalysts. The Au and Ru contents of the catalysts were determined by atomic absorption spectroscopy.

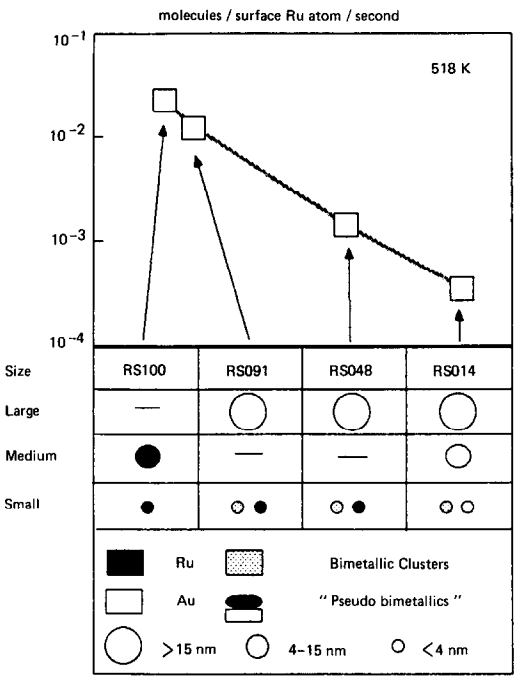

FIG. 8. Relationship between methanation activity and catalyst morphology for the SiO_2-supported catalysts.

performed a detailed examination of the catalyst morphology using analytical electron microscopy (*14, 33*). Figure 8 summarizes our observations concerning the composition of particles in a given particle size range and their relationship to catalyst activity on the SiO_2 series. A clear bimodal particle size distribution was observed. All the large particles were, without exception, monometallic Au particles. These large Au particles seem to be very weakly attached to the SiO_2 support. In fact, during specimen preparation for electron microscopy involving sonication of catalyst powder in isopropanol some of the large Au particles got dislodged from the SiO_2 support and migrated onto the carbon film of the microscope grids. To prevent any bias in the microscopy results, we avoided the sonication technique and resorted to simple grinding of the sample in isopropanol. EDS analysis proved that all the Ru in bimetallic SiO_2-supported catalysts was located exclusively in small particles. These small particles could not be analyzed individually using the JEOL TEM/STEM machine. The individual analysis of these small particles, however, was possible using a dedicated STEM equipped with a field emission gun as the electron source. Most of the particles in this small size range were found to be predominantly Ru, with some of them containing also a trace of Au. To get a better picture of the surface composition of these particles we compared the surface average particle diameter observed by electron microscopy with average particle diameters calculated from hydrogen chemisorption data. Irreversible H_2 chemisorption titrates only Ru sites and does not count Au sites under our conditions. If the Ru was present in the form of monometallic particles, an average particle size between 3 and 4 nm would be expected in the SiO_2 series based on the chemisorption gas uptakes (*14*). The microscopy results show instead that the surface average particle diameter is in the range 1.7–2.6 nm on the SiO_2-supported bimetallics (RS091 and RS048). This discrepancy suggests that part of the surface of the Ru must be diluted by Au, in agreement with the EDS analysis results where Ru was found in conjunction with only a trace of Au in the small particles. Such a hypothesis is also supported by the results of the stepwise H_2/O_2 titration which allows a determination of Au dispersions (*24*). The Au dispersion found was much much higher than expected based on WAXS, and the virtual absence of small, monometallic Au particles according to the EDS analysis of catalysts RS091 and RS048 suggests that the highly dispersed Au must, at least in part, be on the surface of Ru. The drop in the catalytic activity on the SiO_2 series can be correlated with the presence of Au along with Ru in form of small bimetallic clusters (Fig. 8).

On MgO, the situation is much more complex (Fig. 9). Ru was present in small, medium, as well as large particles. The EDS analysis showed that the large parti-

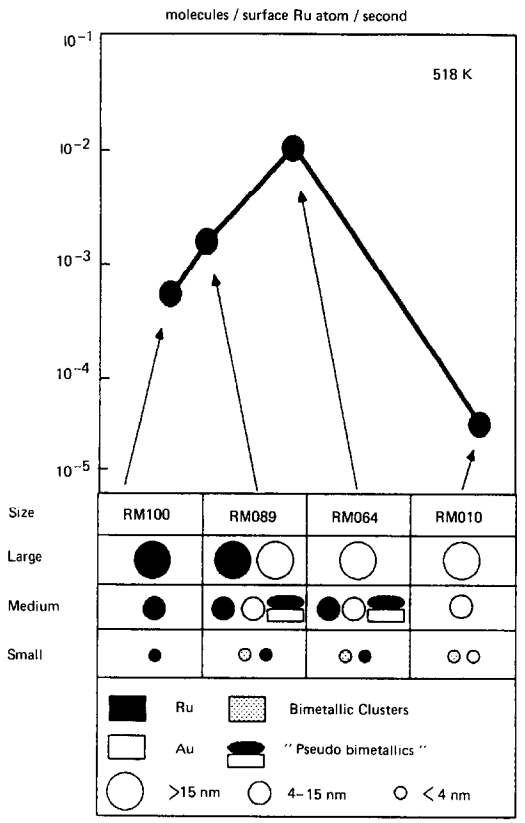

FIG. 9. Relationship between methanation activity and catalyst morphology for the MgO-supported catalysts.

cles were always monometallic, containing either Au or Ru. As regards the small sized particles in the MgO series, they seem to contain predominantly Ru with an occasional trace of Au similar to what was seen on the SiO_2 series. There is, however, an important difference between the MgO and the SiO_2 series, namely the distribution of particle sizes. Due to the higher dispersion of Ru in the SiO_2-supported catalysts, most of the Ru surface area is provided by particles in the small-size range (Figs. 10a and b). On the MgO series, the average particle size is much greater and the main contribution to the available Ru surface area is made by particles in the intermediate-size range (Figs. 11a and b). Thus, while in the SiO_2 series the catalytic action took place predominantly on the small particles, the behavior of the MgO series can only be understood by looking at the particles in the intermediate-size range.

In the medium-size range on Ru–Au/MgO, besides the monometallic particles numerous other particles were found which gave rise to signals for Ru and Au. The analysis of these particles showed significant amounts of both metals to be present; there was, however, no preferred composition. Particles in this size range (10 nm) are likely to be subject to the bulk miscibility constraints which dictate complete immiscibility and phase segregation of the two components (*34*). Thus, we suspect that the particles in the medium-size range consist of one metal which is deposited on top of the other in the form of a three-dimensional overgrowth. A temperature-programmed reduction study showed that in the MgO series, Au nucleated first while Ru was reduced later during catalyst pretreatment in H_2 (*35*). This would allow the Ru to fall either on top of MgO or Au particles. Support for this model comes from a comparison of WAXS data with the Au dispersion measurements derived from stepwise H_2/O_2 titration. WAXS would be able to probe most of the Au particles due to the relatively large Au particle size, and would also account for Au buried underneath Ru. The latter fraction of Au would be inaccessible to gas chemisorption resulting in a gas uptake lower than expected based on WAXS. Such a reduced gas uptake was indeed found experimentally (*24*). A Ru–Au composite particle containing Ru deposited on top of Au cannot be regarded as a bimetallic cluster in a strict sense because the phase segregation of the two metals would keep the surface structure, and thus the catalytic behavior of the individual metal components, unaltered. Hence we have used the term "pseudo-bimetallics" for these medium-size bimetallic particles on MgO. The catalytic activity of the "pseudo-bimetallics" can best be judged by looking at the activity of catalyst RM064. In this sample the largest contribution to the Ru surface area

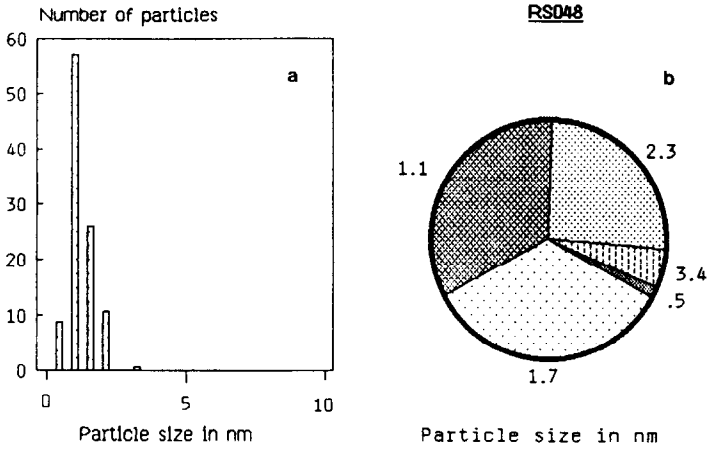

FIG. 10. (a) Particle size distribution on catalyst RS048. (b) Relative contribution to metal surface area by particles in a given size range.

comes from medium-size particles (Fig. 11), and electron microscopy showed that the majority of these particles contained both metals. Surprisingly, this catalyst showed an enhanced activity compared to RM100 (Fig. 9).

The question now arises as to why the activity of Ru increases as one goes from RM100 to RM064. Depending on the catalyst preparation conditions, MgO can exert a negative support-effect suppressing the activity of Ru. This phenomenon has been observed earlier (*31, 35, 36*). The activity of RM100 is significantly lower than that of unsupported Ru sponge (Fig. 12). As seen in Fig. 12, the activity of RM064 approaches the activity of unsupported Ru and RS100 consistent with our model which postulates that a large fraction of Ru in this catalyst is actually "supported" on inert Au rather than on MgO. The presence of Au seems to counteract the support effect of MgO and to partially restore the true behavior of Ru metal. The same principles seem to be at work in RM089 although to a lesser extent.

On catalyst RM010, where we see a drop in the activity, micrographs indicated a

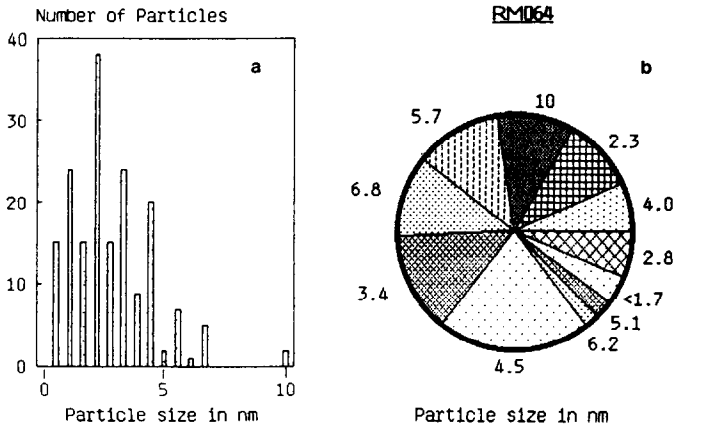

FIG. 11. (a) Particle size distribution on catalyst RM064. (b) Relative contribution to metal surface area by particles in a given size range.

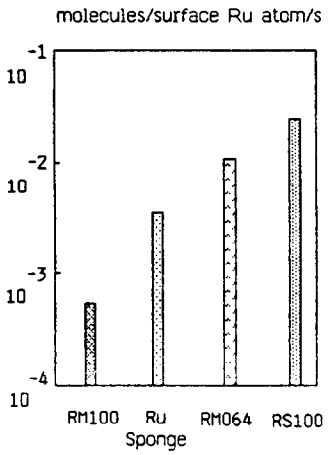

FIG. 12. Effect of support on the specific activity of Ru for methanation. Temperature 518 K; pressure 198 kPa; H_2/CO ratio = 3.

morphology reminiscent of the SiO_2-supported catalysts. There is again a total absence of medium- and large-sized Ru particles, and all the Ru is located in small particles, some of them probably true bimetallic clusters (*14*).

The differences in the particle morphologies on the two catalyst series can be related to the nature of the support and its interaction with the precursor compounds during catalyst preparation. The precursor $RuCl_3$ stays in solution in an acidic medium while it precipitates out in a basic environment. SiO_2 which is acidic and has a high surface area allows a gradual deposition of Ru favoring higher Ru dispersions. The interaction between Au and SiO_2 is weak, leading to a greater mobility of Au. If SiO_2 is coimpregnated with both Ru and Au, the reduction of both metals seems to occur simultaneously. This increases the probability of contact between the two nucleating species allowing bimetallic cluster formation.

In contrast, MgO which is basic in nature and has a low surface area, facilitates precipitation of Ru from the precursor compound. This makes it difficult to achieve high Ru dispersions starting from aqueous preparations (*38*). Furthermore, MgO is unique insofar as it can undergo massive surface area changes during catalyst preparation in aqueous medium (*39*). Au interacts strongly with MgO and thereby has a lower mobility compared to Au/SiO_2. During coimpregnation of MgO, Au seems to get reduced to the metallic state prior to Ru. Ru is deposited later, some of it falling on MgO, and some of it on top of Au. However, in the latter case the two metals are phase-segregated "pseudo-bimetallics" and do not represent true bimetallic clusters.

CONCLUSIONS

In the Ru–Au system, the effect of Au manifests itself primarily through a detrimental influence on the Fischer–Tropsch activity. This effect seems to be predominantly geometric in nature rather than electronic, since Au affects the preexponential factor and not the apparent activation energy for methanation. Further, infrared spectroscopy of adsorbed CO on the bimetallics did not reveal significant shifts in band position compared to the spectra of CO adsorbed on monometallic Ru (*10, 32*) indicating that the electron density of Ru is not altered in any major way.

Striking similarities are seen in the activity patterns in CO hydrogenation and in the structure-sensitive hydrogenolysis of ethane. Small amounts of inactive components such as Au (*13*) or Cu (*19*) on the surface of Ru can lead to a massive drop in turnover numbers for ethane hydrogenolysis due to a dilution of Ru ensembles required for this structure-sensitive reaction. The decline in turnover numbers even in the methanation reaction suggests a comparable ensemble size requirement for both reactions. The methanation and Fischer–Tropsch reactions appear to respond to the presence of Au on the surface of Ru in a manner analogous to that in the ethane hydrogenolysis. The data on Ni–Cu (*17*) and on Ru–Cu (*18*) point in the same direction. Since in the $Ru–Au/SiO_2$ system, the average particle size is not yet in the regime where Kellner

and Bell (*21*) found a massive influence of dispersion on methanation activity ($D >$ 70%), dispersion effects cannot account for the observed drop in the activity.

The Ru–Au bimetallic catalysts do not yield any unusual products compared to monometallic Ru. Apparently, the increased oxygen mobility in MgO due to interactions with Au (*7*) does not play an important role under Fischer–Tropsch synthesis conditions. The complete absence of oxygenated products further suggests that weakly adsorbed CO species on Au sites or on Au^{+1} sites, if any, do not contribute to the reaction in a manner similar to that seen on Pd catalysts. Changes in the olefin/paraffin ratio are dominated by dispersion effects rather than the presence of Au. Our study vividly demonstrates the difficulty in modifying the Fischer–Tropsch product distributions on Ru via secondary components that are by themselves inactive in the synthesis reaction.

During catalyst preparation, the interactions of the precursor compounds with the support have a major influence on the resulting structure and morphology of the catalyst. On SiO_2 we see a bimodal size distribution with large particles containing, without exception, monometallic Au, and all the Ru being located in small particles. Bimetallic cluster formation seems to occur only in the realm of small particles (<3 nm). The evidence obtained from electron microscopy when used in conjunction with chemisorption and WAXS suggests that the Au in these particles may be confined to the surface of the Ru in agreement with the model suggested previously by Sinfelt (*19*). On MgO, on the other hand, Ru exists in large, medium, as well as small particles with bimetallic particles existing in both the medium- and small-size ranges. We tend to believe that the medium-sized bimetallic particles are phase-segregated "pseudo-bimetallics" and not true "bimetallic clusters." The activity trends in both hydrogenolysis and Fischer–Tropsch reactions can be correlated quite well with the distribution of Ru and Au among particles differing in size, structure, and composition.

ACKNOWLEDGMENTS

The authors would like to thank Dr. Lawrence F. Allard, Jr., for his helpful suggestions concerning the microscopy work, and Ms. M. Mochel for performing the STEM-EDS analysis at the University of Illinois. Financial support from NSF through Grant CPE 8212473 is gratefully acknowledged.

REFERENCES

1. Vannice, M. A., *J. Catal.* **37,** 449, 462 (1975).
2. Dry, M. E., *in* "Catalysis Science and Technology" (J. R. Anderson and M. Boudart, Eds.), Vol. I, p. 159. Springer-Verlag, Berlin, 1982.
3. Bassi, I. W., Lytle, F. W., and Parravano, G., *J. Catal.* **42,** 139 (1976).
4. Galvagno, S., and Parravano, G., *J. Catal.* **55,** 178 (1978).
5. Bassi, I. W., Garbassi, F., Vlaic, G., Marzi, A., Tauszik, G. R., Cocco, G., Galvagno, S., and Parravano, G., *J. Catal.* **64,** 405 (1980).
6. Shastri, A. G., Datye, A. K., and Schwank, J., *J. Catal.* **87,** 265 (1984).
7. Schwank, J., Galvagno, S., and Parravano, G., *J. Catal.* **63,** 415 (1980).
8. Poutsma, M. L., Elek, L. F., Ibarbia, P. A., Risch, A. P., and Rabo, J. A., *J. Catal.* **52,** 157 (1978).
9. Yates, D. J. C., *Colloid Interface Sci.* **29,** 194 (1969).
10. Schwank, J., Parravano, G., and Gruber, H. L., *J. Catal.* **61,** 19 (1980).
11. Bulko, J. B., Herman, R. G., Klier, K., and Simmons, G. W., *J. Phys. Chem.* **83,** 3118 (1979).
12. Klier, K., Chatikavani, V., Herman, R. G., and Simmons, G. W., *J. Catal.* **77,** 558 (1982).
13. Galvagno, S., Schwank, J., Parravano, G., Garbassi, F., Marzi, A., and Tauszik, G. R., *J. Catal.* **69,** 283 (1981).
14. Datye, A. K., and Schwank, J. "Proceedings, 8th International Congress on Catalysis, Berlin (West), 1984," Vol. IV, p. 587. Verlag Chemie, Weinheim, 1984.
15. Kelley, R. D., and Goodman, D. W., *Surf. Sci.* **123,** L743 (1982).
16. Goodman, D. W., *Surf. Sci.* **123,** L679 (1982).
17. Bond, G. C., and Turnham, B. D., *J. Catal.* **45,** 128 (1976).
18. Luyten, L. J. M., v. Eck, M., v. Grondelle, J., and v. Hooff, J. H. C., *J. Phys. Chem.* **82,** 2000 (1978).
19. Sinfelt, J. H., *J. Catal.* **29,** 308 (1973).
20. Sinfelt, J. H., "Advances in Catalysis," Vol. 23, p. 91. Academic Press, New York, 1973.
21. Kellner, C. S., and Bell, A. T., *J. Catal.* **75,** 251 (1982).

22. Vannice, M. A., and Twu, C. C., *J. Catal.* **82,** 213 (1983).
23. McIlwrick, C. R., and Phillips, C. S. G., *J. Phys. E* **20,** 1208 (1973).
24. Datye, A. K., Lee, J. Y., Shastri, A. G., and Schwank, J., AIChE 77th Annual Meeting, San Francisco, Calif. Nov. 1984.
25. Satterfield, C. N., and Huff, G. A., *J. Catal.* **73,** 187 (1982).
26. Pannell, R. B., Kibby, C. L., and Kobylinski, T. P., *in* "Proceedings, 7th International Congress on Catalysis, Tokyo, 1980" (T. Seiyama and K. Tanabe, Eds.), p. 447. Elsevier, Amsterdam/Oxford/New York, 1981.
27. Dalla Betta, R. A., Piken, A. G., and Shelef, M., *J. Catal.* **40,** 173 (1975).
28. King, D. L., *J. Catal.* **51,** 386 (1978).
29. Amelse, J. A., Schwartz, L. H., and Butt, J. B., *J. Catal.* **72,** 95 (1981).
30. Sinfelt, J. H., *Acc. Chem. Res.* **10,** 15 (1977).
31. Galvagno, S., Schwank, J., Gubitosa, G., and Tauszik, G. R., *J. Chem. Soc. Faraday Trans. 1* **78,** 2509 (1982).
32. Datye, A. K., Ph.D. thesis, University of Michigan, Ann Arbor, Michigan, 1984.
33. Datye, A. K., Allard, L. F., Jr., and Schwank, J., "Proceedings, 4th Analytical Electron Microscopy Workshop." Lehigh, July 1984.
34. Hansen, M., and Anderko, K., "Constitution of Binary Alloys," 2nd ed., p. 230. McGraw–Hill, New York, 1958.
35. Tauszik, G. R., Leofonti, G., and Galvagno, S., *J. Molec. Catal.* **25,** 357 (1984).
36. Morris, S. R., Moyes, R. B., and Wells, P. B., *in* "Metal-Support and Metal-Additive Effects in Catalysis" (B. Imelik, *et al.*, Eds.), p. 247. Elsevier, Amsterdam, 1982.
37. Bossi, A., Garbassi, F., Orlandi, A., Petrini, G., and Zanderighi, L., *Stud. Surf. Sci. Catal.* **3,** 405 (1979).
38. Murell, L. L., and Yates, D. J. C., *Stud. Surf. Sci. Catal.* **3,** 307 (1979).
39. Leofanti, G., Solari, M., Tauszik, G. R., Garbassi, S., Galvagno, S., and Schwank, J., *Appl. Catal.* **3,** 131 (1982).